JUSTC

Article

http://justc.ustc.edu.cn

Received: April 03, 2023; Accepted: May 30, 2023

Polymerized small molecular dyes providing nanoparticles with stable photosensitivity for eradicating cancer cells

Xu Chen, Feng Gao ✉, and Lihua Yang ✉

Hefei National Research Center for Physical Sciences at the Microscale, CAS Key Laboratory of Soft Matter Chemistry, School of Chemistry and Materials Science, University of Science and Technology of China, Hefei 230026, China

✉Correspondence: Feng Gao, E-mail: gf199203@mail.ustc.edu.cn; Lihua Yang, E-mail: lhyang@ustc.edu.cn

Graphical abstract

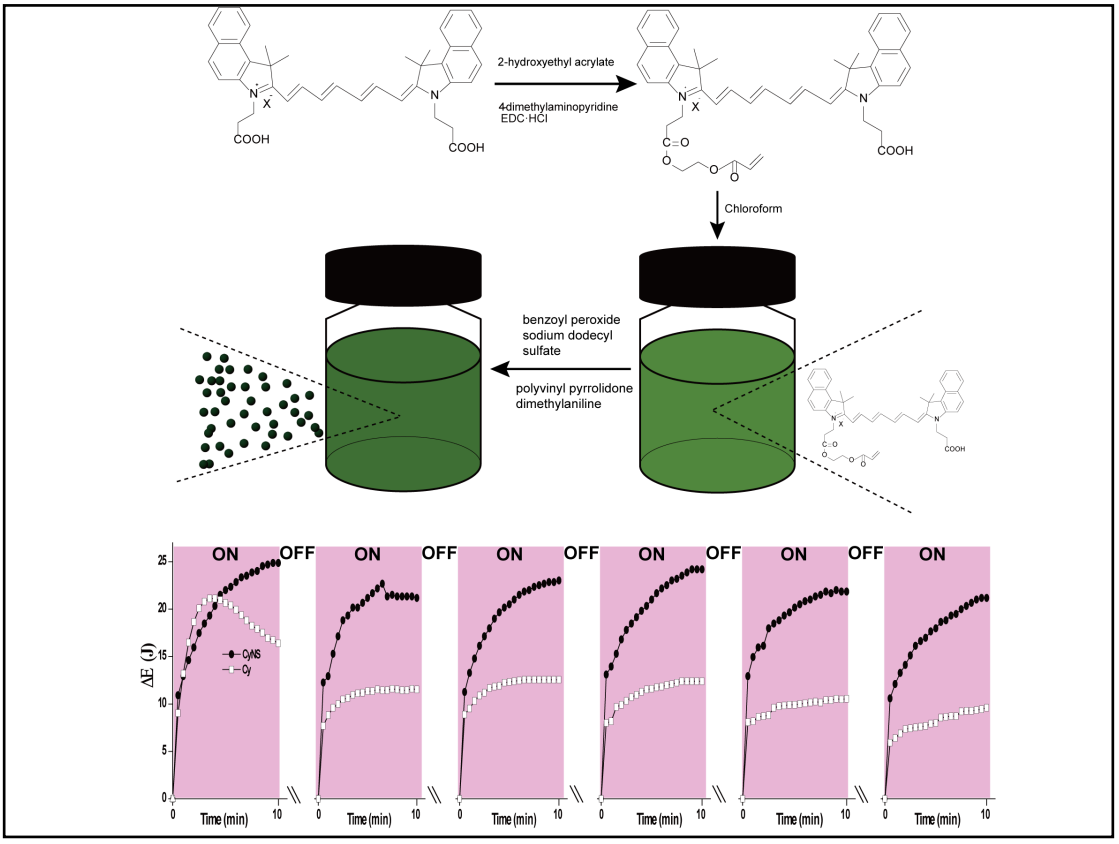

Synthesis route of CSNP and characterization of its photothermal properties.

Public summary

- In order to improve the loading rate of photosensitizer, small molecular dyes were polymerized into nanoparticles by emulsion polymerization, and their photostability was improved by ensuring high loading efficiency of photosensitizer.
- The experimental results show that Cypate nanosphere (CyNS) shows good colloidal stability in PBS and continuous absorption of excitation light.
- After repeated light irradiation, CyNS significantly enhances the stability of photothermal and photodynamic effects, which can lead to a significant improvement in the efficacy of cancer phototherapy with repeated light irradiation.

Citation: Chen X, Gao F, Yang L H. Polymerized small molecular dyes providing nanoparticles with stable photosensitivity for eradicating cancer cells. *JUSTC*, **2023**, 53(6): 0607. DOI: 10.52396/JUSTC-2023-0056

JUSTC

Article

http://justc.ustc.edu.cn

Received: April 03, 2023; Accepted: May 30, 2023

Polymerized small molecular dyes providing nanoparticles with stable photosensitivity for eradicating cancer cells

Xu Chen, Feng Gao ✉, and Lihua Yang ✉

Hefei National Research Center for Physical Sciences at the Microscale, CAS Key Laboratory of Soft Matter Chemistry, School of Chemistry and Materials Science, University of Science and Technology of China, Hefei 230026, China

✉Correspondence: Feng Gao, E-mail: gf199203@mail.ustc.edu.cn; Lihua Yang, E-mail: lhyang@ustc.edu.cn

Cite This: *JUSTC*, **2023**, 53(6): 0607 (8pp)

Read Online

SI Supporting Information

Abstract: To make small molecular photosensitizer-based nanoparticles photostable, we polymerized such photosensitizers via emulsion polymerization, and the resulting nanoparticles exhibited sustained absorption of the excitation wavelength in the near-infrared region, generated stable photothermal and photodynamic effects upon repeated irradiation with an near-infrared laser, and efficiently eradicated cancerous cells even after prior irradiation exposure.

Keywords: photosensitizer; near-infrared; photothermal; photodynamic; cancerous cells

CLC number: TB383; R454 **Document code:** A

1 Introduction

Phototherapy offers spatiotemporally controlled tumor treatment with minimal invasiveness[1–5]. In general, phototherapy comprises two treatment modalities: photothermal therapy[6] and photodynamic therapy[7]. Photothermal therapy ablates tumor cells with the rapid localized heating generated by photothermal agents upon light irradiation[1,8], while photodynamic therapy ablates tumor cells with reactive oxygen species (ROS) generated by photodynamic agents[9] through light-triggered energy transfer from the photosensitizer to surrounding oxygen molecules[7]. Clearly, for both photothermal and photodynamic modalities, a photosensitizer (PS) excitable by an externally applied light source is essential.

Near-infrared light (NIR, 650–900 nm) has maximal transmissivity in tissues and blood[10,11]. Therefore, to achieve deep tissue penetration and minimize heating of nontargeting tissues, phototherapy generally prefers NIR light as the excitation light. Among diverse photosensitizers excitable by NIR light, cyanine dyes, including indocyanine green (ICG)[12–15] and Cypate[16–18], are small organic molecules widely investigated for cancer phototherapy. Indocyanine green, in particular, has been approved by the Food and Drug Administration of the United States. That these small molecular dyes are hydrophobic prompts the development of nanocarriers in which these dyes are preloaded within polymeric micelles or bovine serum albumin self-assembly in efforts to improve their pharmacokinetics[16,17,19]. The resulting nanoparticles, although still excitable by NIR light, exhibit unstable absorption of excitation light — 15-min irradiation is enough to cause ~70% loss in light absorbance[16,17,20]. Strong absorption of the excitation light is a preliminary requirement for promoting phototherapeutic efficacy. It is thus imperative to develop cyanine-dye-preloaded nanosystems that maintain high absorption of excitation light and consequently sustained photothermal and/or photodynamic effects.

Photobleaching of encapsulated cyanine dyes may account for the instability in photosensitivity of the aforementioned nanoparticles. Increasing the loading efficiency of cyanine dyes to an extent well above what is in the aforementioned nanoparticles (generally <20%)[16,17,19,20] may provide a reservoir to counteract the photobleaching effects, which may help maintain the strong absorption of excitation light necessary for achieving sustained photothermal and/or photodynamic effects. To this end, we herein propose to polymerize monomers with cyanine dyes as side groups into nanoparticles via an emulsion polymerization process — an approach that guarantees a PS loading efficiency of >80% — in an effort to achieve photostable dye-preloaded nanoparticle therapeutics.

As a proof-of-concept, we polymerized a dye-appended monomer, in which only one carboxyl group of Cypate (Cy) is esterified with 2-hydroxyethyl acrylate (HEA), into a Cypate-based nanosphere (CyNS) via an emulsion polymerization process. The resulting CyNS nanoparticle retains ~65% absorbance after 15 min of NIR irradiation, leading to sustained generation of photothermal and photodynamic effects after repeated NIR irradiation. This work suggests polymerizing small molecular photosensitizers as an effective pathway toward organic nanoparticles with stable photosensitivity for cancer phototherapy.

2 Materials and methods

2.1 Materials

1,1,2-Trimethyl-1H-benzo[e]indole and N,N-diisopropylethylamine were purchased from 9 Ding Chemistry (Shanghai, China). 1-(3-Dimethylaminopropyl)-3-ethylcarbodiimide

DOI: 10.52396/JUSTC-2023-0056

JUSTC, **2023**, 53(6): 0607

hydrochloride (EDC·HCl), 4-dimethylaminopyridine (DMAP), and N-[5-(phenylamino)-2,4-pentadienylidene] aniline monohydrochloride were purchased from Aladdin (Shanghai, China) and used as received. 2-Hydroxyethyl acrylate (HEA) was purchased from Alfa Aesar (Tianjin, China); dichlorofluorescin diacetate (DCFH-DA) and Cell Counting Kit-8 (CCK-8) were purchased from Beyotime (Shanghai, China). Dulbecco's modified Eagle's medium (DMEM) and fetal bovine serum (FBS) were purchased from HyClone. Acetic anhydride (Ac_2O), sodium acetate, 3-bromopropionic acid, polyvinyl pyrrolidone (PVP, ~40,000 Da), benzoyl peroxide (BPO), sodium dodecyl sulfate (SDS), and dimethylaniline were purchased from Sinopharm Chemical Reagent Co. Ltd. (Shanghai, China). Other reagents used in this work were purchased from Sinopharm Chemical Reagent Co. Ltd. and used as received unless specified otherwise. N,N-dimethylformamide (DMF) and dichloromethane were used with further purification by distillation.

2.2 Preparation of Cypate

Cypate (i.e., Cy) was prepared with a previously reported procedure (Scheme S1)[21,22]. Briefly, 1,1,2-trimethyl-1H-benzo[e]indole (7.51 g, 35.88 mmol) and 3-bromopropanoic acid (8.25 g, 53.93 mmol) were mixed in 1,2-dichlorobenzene (33 mL), and the resulting mixture was heated in an oil bath at 110 °C for 12 h and then cooled to room temperature. The precipitate was collected via filtration, washed with a mixture of acetonitrile: diethyl ether (1∶1, v∶v), and subsequently dried under vacuum, which yielded product 1 (i.e., 1,1,2-trimethyl-1H-benzo[e]indole-3-propanoic acid) as a light gray powder.

A solution of Ac_2O (1.14 g, 11.17 mmol) in dichloromethane (8 mL) was added dropwise to a precooled (at 0–4 °C) solution of N-[5-(phenylamino)-2,4-pentadienylidene] aniline monohydrochloride (2.71 g, 9.52 mmol) and N,N-diisopropylethylamine (2.47 g, 19.11 mmol) in dichloromethane (38 mL) under rigorous stirring with a magnetic bar. The resulting clear solution was stirred for another 1 h and subsequently added dropwise to a refluxing solution of 1,1,2-trimethyl-1H-benzo[e]indole-3-propanoic acid (7.80 g, 21.54 mmol) and sodium acetate (3.04 g, 37.06 mmol) in a mixture of acetonitrile:water = 180.5∶9.5 (v∶v) (190 mL). The resulting mixture was refluxed for 16 h (oil bath at 90 °C), cooled naturally to room temperature, and the precipitate was collected via filtration and then washed successively with acetonitrile, 5% HCl solution, and ethyl ether, which after drying under vacuum yielded purified Cypate as a brown powder.

The ^{1}H nuclear magnetic resonance (NMR) spectrum (AC-250, Bruker) (Fig. S1) confirmed the successful preparation of Cypate. ^{1}H NMR (DMSO-d_6, ppm): 8.4–7.4 (15H, H on beno[e]indol and –CH=CH–CH=CH–CH=CH–CH=), 6.6–6.4 (4H,–CH=CH–CH=CH–CH=CH–CH=),4.42(4H,–CH_2–CH_2–CO–), 2.78 (4H, –CH_2–CH_2–CO–), 1.91 (12H, –CH_3).

2.3 Preparation of Cypate-HEA

Briefly, Cypate (2.02 g, 3.23 mmol) prepared above was dissolved in dry DMF (25 mL), and the resulting solution was then cooled to 0 °C, followed by successive addition of 2-hydroxyethyl acrylate (3 g, 25.84 mmol) and 4-dimethylaminopyridine (0.079 g, 0.65 mmol) and then addition (dropwise) of a solution of EDC·HCl (1.24 g, 6.47 mmol) in dichloromethane (45 mL). The resulting mixture was stirred at room temperature for 72 h and concentrated successively via rotary evaporation to remove dichloromethane and under a relatively higher vacuum provided by an oil pump to remove most of the DMF. The resultant thick green liquid was subsequently precipitated in DI water (1 L) with stirring, and the resulting precipitate was collected via filtration, dried under vacuum, and purified by flash column chromatography using dichloromethane:methanol (9∶1 v/v) as the eluent, which after rotary evaporation and lyophilization yielded the Cypate-HEA product as a dark green solid.

The ^{1}H nuclear magnetic resonance (NMR) spectrum (AC-250, Bruker) (Fig. S2) confirmed the successful preparation of Cypate-HEA. ^{1}H NMR (DMSO-d_6, ppm): 8.4–7.4 (15H, H on beno[e]indol and –CH=CH–CH=CH–CH=CH–CH=), 6.7–5.8 (7H, –CH=CH–CH=CH–CH=CH–CH=, –CH=CH_2), 4.42 (4H, –CH_2–CH_2–CO–), 4.26 (4H, –O–CH_2–CH_2–O–), 2.9–2.7 (4H, –CH_2–CH_2–CO–), 1.91 (12H, –CH_3).

2.4 Synthesis of Cypate nanosphere (CyNS)

Cypate nanospheres were synthesized via an emulsion polymerization process. A magnetic bar, solution of Cypate-HEA monomer (5 mg) in chloroform (180 μL), solution of benzoyl peroxide (0.1 mg) in chloroform (10 μL), and solution of sodium dodecyl sulfonate (0.1 g) and polyvinyl pyrrolidone (0.2 g) codissolved in water (10 mL) were successively added to a flat-bottom vial. The resulting mixture was sonicated (at an output power of 90 W) for 20 min, and the vial was subsequently sealed with parafilm and then filled with nitrogen (through a 5-min N_2 flow), followed by the addition of dimethylaniline (0.25 mg) in chloroform (10 μL) (by puncturing a small hole through the parafilm seal) and sealing with the lid. The vial was then stirred at room temperature under rigorous stirring (600 r/min), and the precipitate was collected via centrifugation (12,000 g, 10 min), washed with Millipore water three times, and redispersed in Millipore water, which yielded a CyNS dispersion in water as a dark green dispersion.

2.5 Characterizations of CyNS

The morphology of CyNS was characterized using a transmission electron microscope (TEM) (H-7650, Hitachi) operated at 100 kV; prior to TEM characterizations, one drop of a CyNS suspension was added onto a carbon-coated copper grid and dried under ambient conditions, followed by TEM imaging. The hydrodynamic diameter and zeta potential of CyNS (10 μg/mL PS dosage) were measured using a nanoparticle analyzer (Nano-ZS90, Malvern) at 25 °C. UV–vis-NIR absorption spectra of CyNS in aqueous solution were recorded using a UV–vis spectrometer (Cary 60 UV–Vis, Agilent).

2.6 Characterizing the photosensitizer group content for a CyNS stock dispersion

To help quantify the PS group content in a CyNS stock dispersion, the Cypate-HEA calibration curve in DMF was

DOI: 10.52396/JUSTC-2023-0056
JUSTC, **2023**, 53(6): 0607

measured (Fig. S3c–d) by measuring the absorbance at 785 nm (OD_{785}) of Cypate-HEA solution at varying concentrations with a UV–vis spectrometer (Cary 60 UV–Vis, Agilent). To determine the PS group content in a CyNS stock dispersion, we diluted the CyNS stock dispersion in millipore water by ~10 times with DMF and then monitored the OD_{785} of the resulting dilute with a UV –vis spectrometer (Cary 60 UV–Vis, Agilent).

2.7 Test on the stability of absorbing excitation light

A dispersion (0.5 mL) of CyNS containing 10.0 μg/mL PS was irradiated with an 808-nm laser at 1.0 W/cm^2 for 15 min. A solution of free Cypate (10.0 μg/mL, 0.5 mL) in DMF was irradiated similarly. The absorbance at 808 nm (OD_{808}) of these two samples was measured at various time points (i.e., 0, 1, 2, 3, 5, 10, and 15 min) during irradiation using a UV–vis spectrometer (Cary 60 UV–Vis, Agilent).

2.8 Characterization of the in vitro photothermal effects

The in vitro photothermal conversion effects of a CyNS dispersion in PBS (PS content of 10 μg/mL) were characterized by monitoring the temperature rise of the dispersion (400 μL) at different time points during irradiation with an 808-nm laser. Temperature rises of a Cypate solution in DMF (10 μg/mL, 400 μL) during similar treatment were recorded for comparison.

To assess how repeated NIR irradiation affects the stability of photothermal effects generated by CyNS, we subjected a CyNS dispersion (PS content of 10 μg/mL, 400 μL) to the expected number (3 or 6) of irradiation cycles (808-nm laser at 1.0 W/cm^2 for 10 min) and then cooled naturally to room temperature (waiting for 10 min and 12 h after suspending the irradiation for 3 and 6 irradiation cycles, respectively). Similar treatments were performed with a solution of free Cypate in DMF (10 μg/mL, 400 μL) for comparisons.

The as-recorded temperature rises were converted into heat generated via photothermal effects using the function below:

$$\Delta E = c \times m \times \Delta T,$$

where ΔE is the cumulative heat generated via photothermal effects at time-point "t", ΔT is the cumulative temperature rise at time-point "t", c is the specific heat of the solvent (water or DMF), and m is the mass of the solvent.

2.9 Characterization of the in vivo photothermal effects

BALB/c mice bearing 4T1 murine breast tumors were used as a mouse model for characterizing the in vivo photothermal effects. Nine BALB/c female mice (3–4 weeks old) were obtained from the Animal Center of Shanghai and, into their rear flanks, subcutaneously injected with ~3×10^6 4T1 murine breast cancer cells in PBS (100 μL), which after 1–2 weeks of growth yielded 4T1 tumors. These 4T1 tumor-bearing mice were randomly divided into 3 groups (n= 3 per group), and among them, two groups were treated with CyNS in PBS (PS content = 0.5 mg/mL, 100 μL per mouse) and Cypate in PBS (0.5 mg/mL, 100 μL each mouse), and the remaining group was treated with sterile PBS (100 μL each mouse); all injections were administered intratumorally. Immediately after injection, each mouse was irradiated with an 808-nm laser at a power density of 1 W/cm^2 for 10 min, during which thermographs were recorded with an infrared thermal camera as a function of irradiation time. All animal experiments were conducted in compliance with the guidelines for the care and use of research animals established by the Animal Care and Use Committee at the University of Science and Technology of China.

2.10 Characterization of the in vitro photodynamic conversion

We assessed whether a dispersion of CyNS in PBS and a solution of free Cypate in methanol exhibit photodynamic effects upon light irradiation by monitoring its ROS generation with an ROS kit that uses dichlorofluorescein diacetate (DCFH-DA) as the ROS-sensitive fluorescent probe[23, 24]. Briefly, 2 mL of 0.01 mol/L NaOH were added to 0.5 mL of 1 mmol/L DCFH-DA in ethanol (Beyotime) and incubated at room temperature for 30 min to hydrolyze DCFH-DA. The resulting hydrolysate, DCFH, was neutralized with 10 mL 1× PBS (pH 7.4) and placed on ice in the dark. One milliliter of 40 μmol/L DCFH was added onto a dispersion of CyNS in PBS and a solution of free Cypate in methanol (both at PS content of 15 μg/mL, 500 μL), followed by 4 cycles of 10-min irradiation with an 808-nm laser (at 1.0 W/cm^2). After each 10-min irradiation dose, fluorescence emission spectra of the resultant solutions were recorded using a fluorometer (F-4600 spectrofluorometer, Hitachi) using an excitation wavelength of 488 nm and emission range of 505–550 nm (with a slit-width of 5 nm for both excitation and emission wavelengths). DCFH in dispersions of CyNS in PBS or Cypate in methanol (15 μg/mL PS dosage, 500 μL) treated under similar conditions but no irradiation served as controls. References are those (i.e., either 500 μL PBS or 500 μL DMF) treated similarly but without photosensitizer addition.

2.11 In vitro cell studies

The in vitro cytotoxicity of CyNS was assessed with Cell Counting Kit-8 (CCK-8) assays using HeLa cells as a representative cancerous cell line. Briefly, approximately 10,000 cells in Dulbecco's modified Eagle's medium (DMEM, SH30022.01B, HyClone) supplemented with 10% fetal bovine serum (FBS) were seeded into a well of 96-well plates, incubated at 37 °C for 24 h, incubated in FBS-absent DMEM with CyNS in PBS (at varying PS content, 100 μL) for 4 h, and subsequently irradiated with an 808-nm laser at 1.0 W/cm^2 for 10 min. Relative cell viabilities were determined by monitoring the optical densities at 450 nm with a microplate reader (Varioskan, Thermo). Controls included those assayed similarly but without laser irradiation to indicate the intrinsic cytotoxicity of CyNS. To further examine how photostability affects in vitro cytotoxicity, we carried out similar CCK-8 assays but with CyNS or Cypate dispersion (PS dosage of 30 μg/mL, 400 μL) pretreated with 5-min irradiation (808-nm laser at 1.0 W/cm^2 and cooled naturally for 1 h). Each trial was carried out in triplicate, and the reported results are averages of two independent trials.

2.12 Statistical analysis

Statistical comparisons were performed via Student's t test

DOI: 10.52396/JUSTC-2023-0056
JUSTC, **2023**, 53(6): 0607

using the statistical software package BioMedCalc (version 2.9), and p values of < 0.05 and < 0.01 were considered indications of significant differences and statistically significant differences, respectively.

3 Results and discussion

3.1 Synthesis and characterization of CyNS

The preparation of CyNS comprises two steps (Scheme 1): preparing the Cypate-HEA monomer in which only one carboxyl group of Cypate is esterified with HEA and polymerizing Cypate-HEA into CyNS via an emulsion polymerization process. Cypate-HEA monomer was prepared by esterifying commercially available HEA monomer with Cypate prepared according to a previously reported procedure[22], followed by removal of residual Cypate and Cypate-HEA monomer in which both carboxyl groups have been esterified, which yielded Cypate-HEA monomer in which only one carboxyl group of Cy is esterified, as confirmed by the proton nuclear magnetic resonance (^{1}H NMR) spectra (Figs. S1–S2). The as-prepared Cypapte-HEA monomer was then polymerized via an emulsion polymerization procedure, which yielded the expected CyNS nanoparticles.

Preparation of CyNS nanoparticles was monitored by characterizing the morphology, size, zeta potential, and optical properties. The as-prepared CyNS nanoparticles are spherical with a size of ~200 nm under transmission electron microscopy (TEM) (Fig. 1a). When dispersed in phosphate buffered saline (PBS), these CyNS nanoparticles exhibit an average hydrodynamic diameter of 220.1 nm ± 2.5 nm (PDI = 0.139) (Fig. 1c). The CyNS nanoparticle size distribution of Cayman nanoparticles is shown in Fig. S3a, with a negative average zeta potential of −16.78 mV ± 0.92 mV (Fig. 1b) in aqueous solution, likely owing to the presence and hydration effects of polyvinyl pyrrolidone (PVP, ~40,000 Da), a stealth biopolymer potentially alternative to polyethylene glycol (PEG)[25] — which is introduced as a stabilizer for nanoparticle formation during the emulsion polymerization procedure. Moreover, the CyNS nanoparticle exhibits good colloidal stability in PBS, as indicated by the negligible increase in hydrodynamic diameter over a span of 5 d (Fig. 1c). UV–vis–NIR absorption spectra reveal that the as-prepared CyNS nanoparticles dispersed in PBS inherit the strong absorption in the near-infrared region characteristic of Cypate (Fig. S3b). Collectively, these results suggest successful preparation of the expected CyNS nanoparticle.

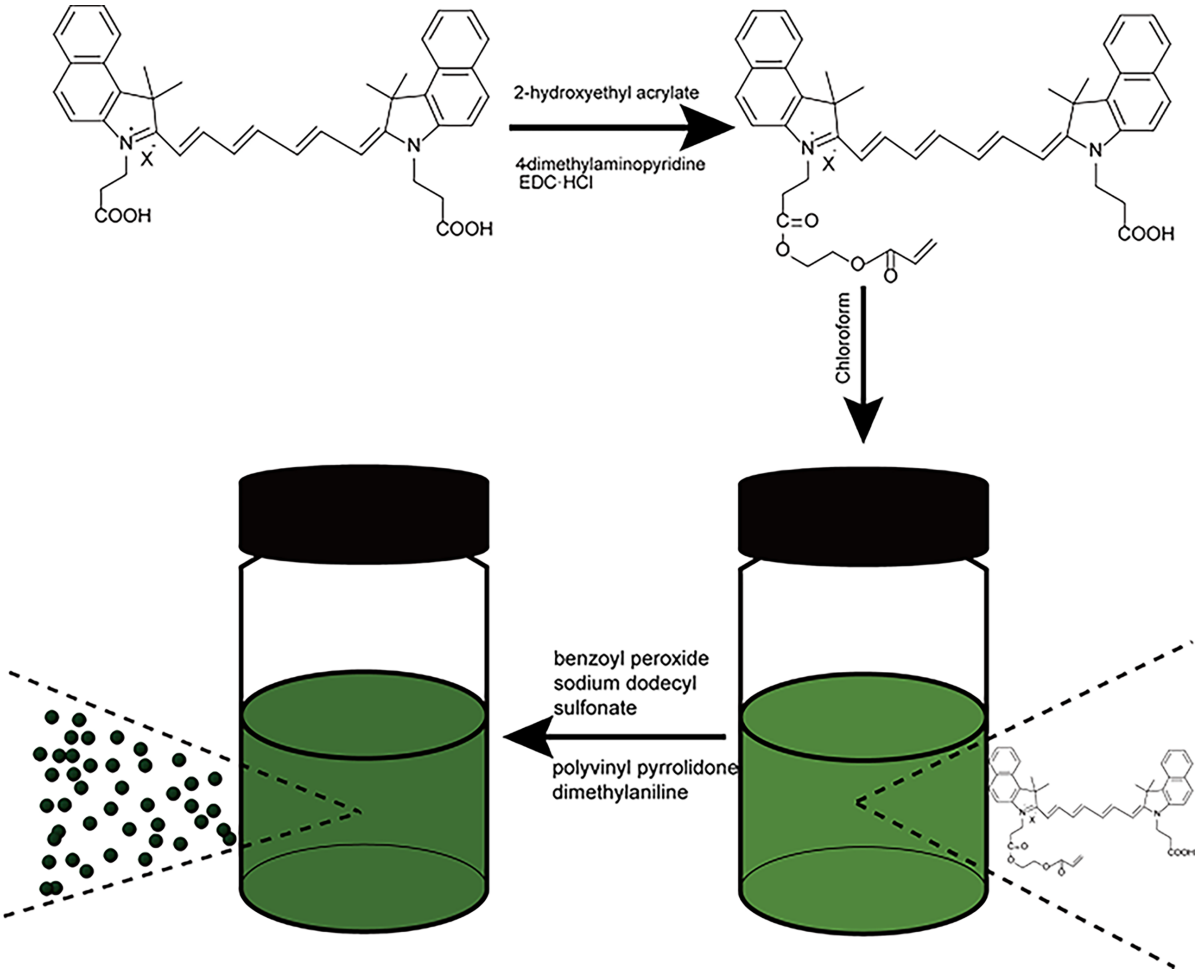

Scheme 1. Schematic illustration of the preparation of Cypate nanospheres (CyNSs), which are obtained by polymerizing the Cypate-HEA monomer, in which one carboxyl group of a Cypate molecule is esterified with 2-hydroxyethyl acrylate (HEA) via an emulsion polymerization process.

DOI: 10.52396/JUSTC-2023-0056
JUSTC, **2023**, 53(6): 0607

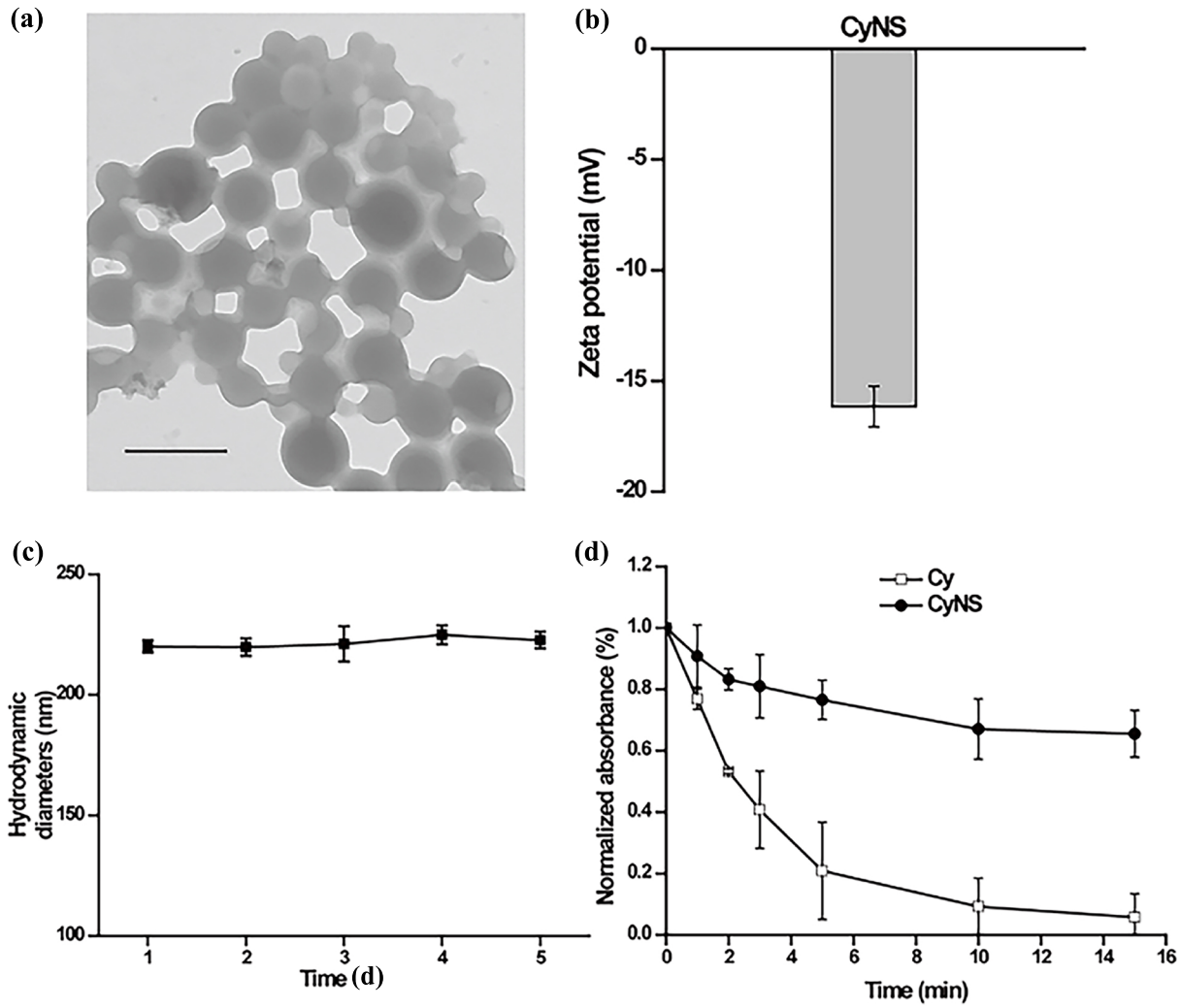

Fig. 1. (a) Transmission electron microscopy image of CyNS. Scale bar = 500 nm. (b) The average zeta potential of CyNS in aqueous solution. (c) The average hydrodynamic diameters of CyNS in 1×PBS over a span of 5 d. Data points are reported as the mean ± standard deviation. (d) Normalized absorbance ratios of CyNS (PS content of 10.0 μg/mL, 0.5 mL) at different time points during irradiation with an 808-nm laser at 1.0 W/cm² for 15 min in total, with those of free Cypate included for comparison.

3.2 Characterization of photothermal and photodynamic properties of CyNS

Sustained absorption of excitation light is a preliminary requirement for achieving efficient and stable photothermal and/or photodynamic effects. To assess whether our CyNS acquires sustained absorption of excitation light, we monitored the absorbance (at 808 nm) of CyNS at different time points during a 15-min irradiation with an 808-nm laser at 1 W/cm², with the performance of free Cypate included as a reference. In contrast to free Cypate, CyNS exhibits very gradual decreases in absorbance during the 15-min irradiation. After the 15-min irradiation, CyNS retains 65% absorbance of its nonirradiated counterpart, compared to the 5% retained absorbance by free Cypate (Fig. 1d), indicative of significantly enhanced photostability, likely owing to the high loading efficiency of the Cypate group within CyNS as well as protection by PVP on the surface of CyNS.

Capable of maintaining high absorption of excitation light, does CyNS generate efficient and stable photothermal and/or photodynamic effects? To address this, we first investigated whether the high loading of Cypate leads to the quenching of the photothermal/photodynamic ability of Cypate. As shown in Fig. S4, as the concentration of Cypate increases, the fluorescence intensity of CyNS does indeed decrease. To ensure that CyNS has good photothermal/photodynamic performance in subsequent experiments, we determined the concentration of Cypate loaded as 10 μg/μL. We characterized the photothermal effects and photodynamic reactions generated by CyNS upon repeated NIR irradiation, with the performance of free Cypate included as a reference. Characterizations of the in vitro photothermal effects (Fig. 2a and Fig. S5) reveal that during one dose of irradiation (808-nm laser at 1.0 W/cm² for 10 min), CyNS generates similar amount of heat as does free Cypate during the first 5-min of irradiation; nevertheless, during the subsequent 5-min irradiation, cumulative heat generated by CyNS continues increasing, whereas that generated by free Cypate has decreased relatively by ~22.3% (Fig. 2a and Fig. S5c). Repeating the same irradiation dose six times (with 12-h natural cooling intervals) makes CyNS generate 14.9% less heat compared to 54.6% less heat generated by free Cypate (Fig. 2a). Obviously, CyNS generates ef-

DOI: 10.52396/JUSTC-2023-0056
JUSTC, **2023**, 53(6): 0607

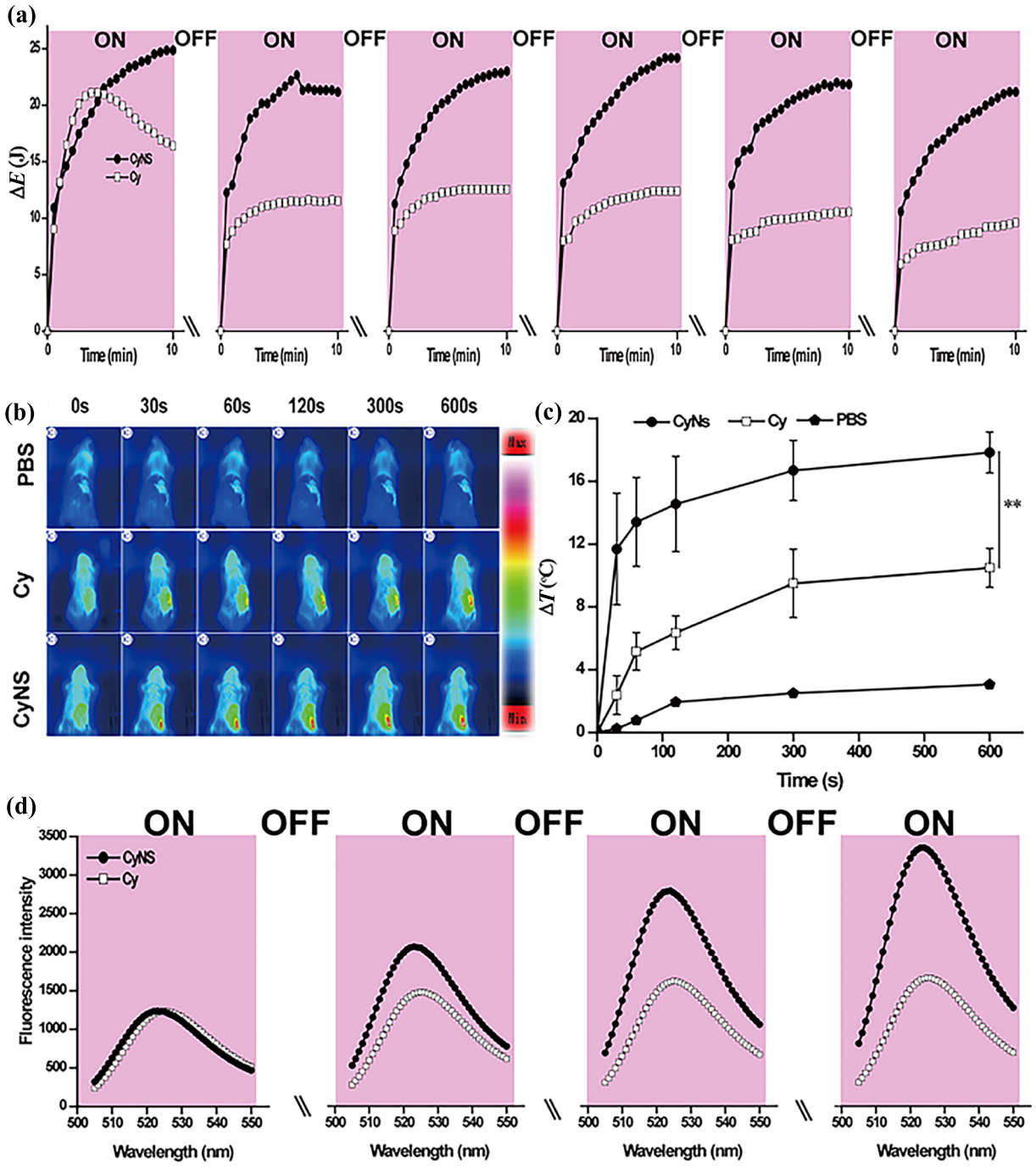

Fig. 2. (a) Cumulative heat generated by the dispersion of CyNS in PBS (PS content of 10 μg/mL, 400 μL) at different time points during the 1st, 2nd, 3rd, 4th, 5th, and 6th irradiation treatments (with an 808-nm laser at 1.0 W/cm² for 10 min), with those of free Cypate in DMF included for comparison. \\: indicates natural cooling for 12 h. (b) Thermographs of mice injected with CyNS, free Cypate, or PBS during a 10-min irradiation (with an 808-nm laser at 1.0 W/cm²) immediately after injection. Mice assayed similarly but injected with PBS only are included as a reference. (c) Plots of temperature change at the tumor site as a function of irradiation time based on thermographs. Data points are reported as the mean ± standard deviation (n=3). ** indicates p< 0.01. (d) Fluorescence emission spectra of dichlorofluorescein hydrolysate (DCFH) in dispersions of CyNS in PBS and Cypate in methanol after the 1st, 2nd, 3rd, and 4th treatments. \\: natural cooling for 2 min.

ficient and stable photothermal effects, whereas free Cypate fails to do so.

3.3 Characterizations of the in vivo photothermal effects

Similar results were observed with characterizations of the in vivo photothermal effects in tumor-bearing mice. To eliminate potential interference due to complex in vivo conditions and thus compare photothermal effects generated CyNS and free Cypate at same dosage of the photosensitizing group (i.e., PS), we pretreat both CyNS and free Cypate with 5-min irradiation (808-nm laser at 1.0 W/cm²), intratumorally inject either of the as-pretreated samples into mice bearing 4T1 tumors (50 μg PS per mouse), and irradiate the mice (808-nm laser at 1.0 W/cm²) immediately after injection with thermal

DOI: 10.52396/JUSTC-2023-0056
JUSTC, **2023**, 53(6): 0607

graphs recorded using an infrared thermal camera (Fig. 2b). During the 10-min NIR irradiation, the average temperature rise at tumor sites of mice treated with CyNS was consistently higher than that of mice treated with free Cypate; after the 10-min irradiation, CyNS generated a temperature rise of 17.8 °C compared to 10.4 °C by free Cypate (Fig. 2c). Note that when the pretreatment (i.e., 5-min NIR irradiation) is not applied, CyNS and free Cypate cause similar temperature rises at tumor sites through the 10-min NIR irradiation (Fig. S7). Therefore, the observed higher temperature rise generated by pretreated CyNS than by the free Cypate counterpart must arise because of CyNS' significantly improved photostability.

Enhancement in the photostability of CyNS is also observed with characterizations of in vitro photodynamic effects (Fig. 2d and Fig. S6d), in which the amount of ROS generated via photodynamic effects is indicated by an increase in the fluorescence intensity of a fluorescent probe. Upon one dose of irradiation (808-nm laser at 1.0 W/cm^2 for 5 min), CyNS consistently caused higher fluorescence intensity than free Cypate, indicative of more ROS generated by CyNS via photodynamic effects. Repeating the same dose of irradiation makes CyNS cause a rapid and significant increase in fluorescence intensity — for example, leading to a >3-fold increase in fluorescence intensity at 525 nm — but fails to do so with free Cypate. Combined with results on in vitro photothermal effects (Fig. 2a and Figs. S5, S6a–c), these results suggest that upon repeated NIR irradiation that simulates the normal irradiation practice in phototherapy, CyNS generates relatively stable photothermal effects and photodynamic reactions, whereas free Cypate fails to do so, suggesting that CyNS may offer better phototherapy efficacy.

More stable in generating photothermal and photodynamic effects, does CyNS necessarily lead to stronger cytotoxicity than free Cypate? To address this, we performed in vitro cell viability assays using HeLa cells as a representative cancer cell line. To help evaluate how photostability impacts photoresponsive cytotoxicity, we pretreated CyNS and free Cypate with 5 min of NIR irradiation and used the as-pretreated sample for subsequent CCK-8 assays. Our results show that CyNS, although barely cytotoxic in the absence of irradiation (Fig. S8a), reduces the cell viability ratio to ~40% upon 10-min NIR irradiation regardless of whether the 5-min pretreatment is applied ($p > 0.05$) (Fig. 3). In contrast, free Cypate, although capable of causing significant cell viability loss upon 10-min irradiation as does CyNS when pretreatment is not superimposed ($p > 0.05$), fails to do so after the 5-min pretreatment is applied (Fig. 3), likely due to its loss of ability to generate photothermal effects after the 5-min pretreatment (Fig. S8b). Collectively, these results suggest that, compared to free Cypate, CyNS, which has strikingly enhanced photostability, may provide significantly improved efficacy during phototherapy in which repeated irradiation is normally applied.

4 Conclusions

In conclusion, we show that polymerizing small molecular dyes into nanoparticles via an emulsion polymerization process is an effective approach to enhance their photostability, likely by guaranteeing extremely high photosensitizer loading efficiency. The resulting nanoparticle exhibits sustained absorption of excitation light and, in doing so, strikingly enhanced stability in generating photothermal and photodynamic effects even after repeated light irradiations, which may lead to significantly improved efficacy in cancer phototherapy in which repeated irradiation is normally applied.

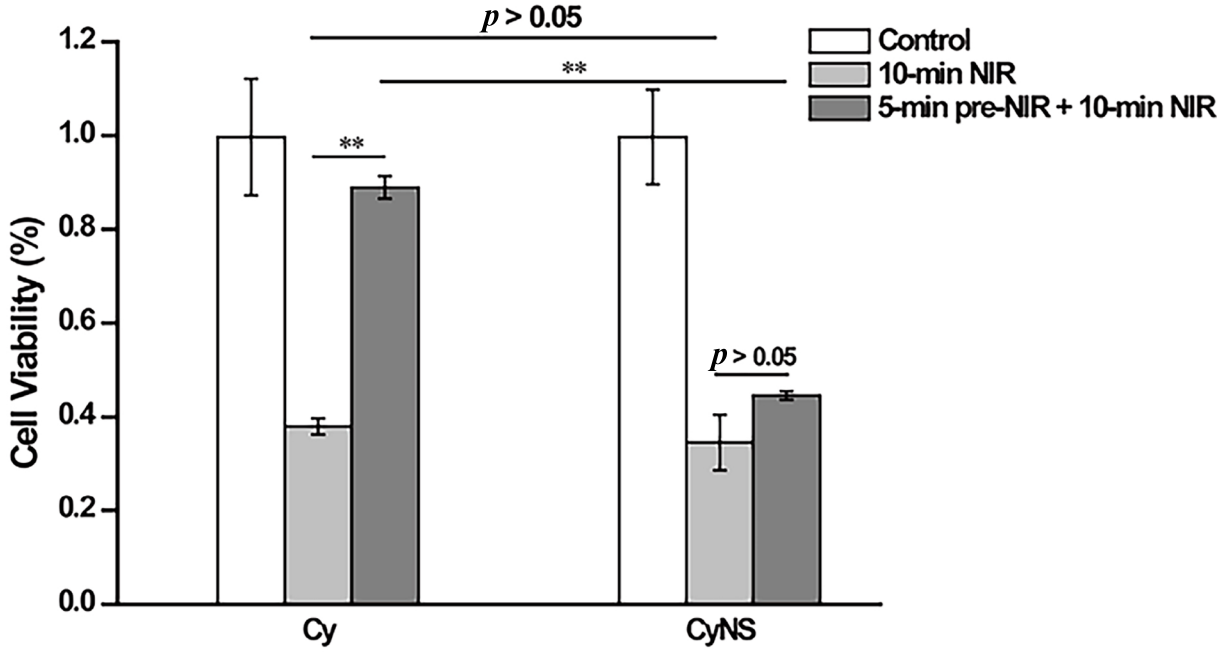

Fig. 3. In vitro cell viability assays using free Cy/pretreated Cy and CyNS/pretreated CyNS incubated with HeLa cells for 24 h with 10 min of irradiation (808 nm, 1.0 W/cm^2). Controls are culture medium irradiated similarly with an 808-nm laser at 1.0 W/cm^2. Data points are reported as the mean ± standard deviation. ** indicates $p < 0.01$.

DOI: 10.52396/JUSTC-2023-0056
JUSTC, **2023**, 53(6): 0607

Supporting information

The supporting information for this article can be found online at https://doi.org/10.52396/JUSTC-2023-0056.

Acknowledgements

This work was supported by the Youth Innovation Promotion Association of the Chinese Academy of Sciences and the Ministry of Education of the People's Republic of China (NCET-13-0547). We gratefully thank Professors Jun Wang and Zhishen Ge for use of their facilities. We also thank Lulu Xu and Jigang Piao for technical assistance.

Conflict of interest

The authors declare that they have no conflict of interest.

Biographies

Xu Chen is currently pursuing a master's degree at the University of Science and Technology of China. His research focuses on the application of nanomaterials in the biological field.

Feng Gao received his Ph.D. degree in Materials Science and Engineering from the University of Science and Technology of China (USTC) in 2021. Currently, he is a postdoctoral fellow at USTC. His research focuses on the preparation of biomaterials and their applications in antibacterial and artificial carbon cycling.

Lihua Yang received her Ph.D. degree from the University of Illinois at Urbana Champaign in 2008. She is currently an Associate Professor at the University of Science and Technology of China. Her research mainly focuses on the application of nanomaterials in the biological field.

References

[1] Yuwen L H, Zhou J J, Zhang Y Q, et al. Aqueous phase preparation of ultrasmall $MoSe_2$ nanodots for efficient photothermal therapy of cancer cells. *Nanoscale,* **2016**, *8* (5): 2720–2726.
[2] Huang P, Lin J, Li W W, et al. Biodegradable gold nanovesicles with an ultrastrong plasmonic coupling effect for photoacoustic imaging and photothermal therapy. *Angew. Chem. Int. Edit.,* **2013**, *52* (52): 13958–13964.
[3] Tian B, Wang C, Zhang S, et al. Photothermally enhanced photodynamic therapy delivered by nano-graphene oxide. *ACS Nano,* **2011**, *5* (9): 7000–7009.
[4] Shi S G, Zhu X L, Zhao Z X, et al. Photothermally enhanced photodynamic therapy based on mesoporous $Pd@Ag@mSiO_2$ nanocarriers. *J. Mater. Chem. B.,* **2013**, *1* (8): 1133–1141.
[5] Huang X H, El-Sayed I H, Qian W, et al. Cancer cell imaging and photothermal therapy in the near-infrared region by using gold nanorods. *J. Am. Chem. Soc.,* **2006**, *128* (6): 2115–2120.
[6] Nolsøe C P, S. Torp-Pedersen S, Burcharth F, et al. Interstitial hyperthermia of colorectal liver metastases with a US-guided Nd-YAG laser with a diffuser tip: A pilot clinical study. *Radiology,* **1993**, *187* (2): 333–337.
[7] Dolmans D E J G J, Fukumura D, Jain R K. Photodynamic therapy for cancer. *Nat. Rev. Cancer,* **2003**, *3* (5): 380–387.
[8] Piao J G, Wang L M, Gao F, et al. Erythrocyte membrane is an alternative coating to polyethylene glycol for prolonging the circulation lifetime of gold nanocages for photothermal therapy. *ACS Nano,* **2014**, *8* (10): 10414–10425.
[9] Chen H C, Tian J W, He W J, et al. H_2O_2-activatable and O_2-evolving nanoparticles for highly efficient and selective photodynamic therapy against hypoxic tumor cells. *J. Am. Chem. Soc.,* **2015**, *137* (4): 1539–1547.
[10] Weissleder R. A clearer vision for in vivo imaging. *Nat. Biotechnol.,* **2001**, *19* (4): 316–317.
[11] Weissleder R, Ntziachristos V. Shedding light onto live molecular targets. *Nat. Med.,* **2003**, *9* (1): 123–128.
[12] Ma Z Y, Yang M K, Foda M F, et al. Polarization of tumor-associated macrophages promoted by vitamin C-loaded liposomes for cancer immunotherapy. *ACS Nano,* **2022**, *26* (10): 17389–17401.
[13] Wu L, Fang S T, Shi S, et al. Hybrid polypeptide micelles loading indocyanine green for tumor imaging and photothermal effect study. *Biomacromolecules,* **2013**, *14* (9): 3027–3033.
[14] Zheng X H, Xing D, Zhou F F, et al. Indocyanine green-containing nanostructure as near infrared dual-functional targeting probes for optical imaging and photothermal therapy. *Mol. Pharmaceut.,* **2011**, *8* (2): 447–456.
[15] Yu J, Javier D, Yaseen M A, et al. Self-assembly synthesis, tumor cell targeting, and photothermal capabilities of antibody-coated indocyanine green nanocapsules. *J. Am. Chem. Soc.,* **2010**, *132* (6): 1929–1938.
[16] Yang H, Mao H J, Wan Z H, et al. Micelles assembled with carbocyanine dyes for theranostic near-infrared fluorescent cancer imaging and photothermal therapy. *Biomaterials,* **2013**, *34* (36): 9124–9133.
[17] Wang Y, Yang T, Ke H T, et al. Smart albumin-biomineralized nanocomposites for multimodal imaging and photothermal tumor ablation. *Adv. Mater.,* **2015**, *27* (26): 3874–3882.
[18] Han Y, Li J J, Zan M H, et al. Redox-responsive core cross-linked micelles based on cypate and cisplatin prodrugs-conjugated block copolymers for synergistic photothermal–chemotherapy of cancer. *Polym. Chem.,* **2014**, *5* (11): 3707–3718.
[19] Zheng M B, Yue C X, Ma Y F, et al. Single-step assembly of DOX/ICG loaded lipid–polymer nanoparticles for highly effective chemo-photothermal combination therapy. *ACS Nano,* **2013**, *7* (3): 2056–2067.
[20] Li Y L, Deng Y B, Tian X, et al. Multipronged design of light-triggered nanoparticles to overcome cisplatin resistance for efficient ablation of resistant tumor. *ACS Nano,* **2015**, *9* (10): 9626–9637.
[21] Bugaj J E, Achilefu S I, Dorshow R B, et al. Novel fluorescent contrast agents for optical imaging of in vivo tumors based on a receptor-targeted dye-peptide conjugate platform. *J. Biomed. Opt.,* **2001**, *6* (2): 122–133.
[22] Ye Y P, Bloch S, Kao J, et al. Multivalent carbocyanine molecular probes: Synthesis and applications. *Bioconjugate Chem.,* **2005**, *16* (1): 51–61.
[23] Bourré L, Thibaut S, Briffaud A, et al. Indirect detection of photosensitizer ex vivo. *J. Photochem. Photobiol. B,* **2002**, *67* (1): 23–31.
[24] Yuan Y, Min Y, Hu Q, et al. NIR photoregulated chemo- and photodynamic cancer therapy based on conjugated polyelectrolyte–drug conjugate encapsulated upconversion nanoparticles. *Nanoscale,* **2014**, *6* (19): 11259–11272.
[25] Knop K, Hoogenboom R, Fischer D, et al. Poly(ethylene glycol) in drug delivery: Pros and cons as well as potential alternatives. *Angew. Chem. Int. Ed.,* **2010**, *49* (36): 6288–6308.

DOI: 10.52396/JUSTC-2023-0056
JUSTC, **2023**, 53(6): 0607